

Post buckling stress state of open section cylindrical shells subjected to constrained torsion

Tomasz Kopecki

Faculty of Mechanical Engineering and Aeronautics, Rzeszów University of Technology,
ul. W. Pola 2, PL 35-959 Rzeszów, POLAND
e-mail: t_kopecki@poczta.wp.pl

SUMMARY

The work concerns numerical and experimental studies on pre and post buckling of thin-walled steel cylindrical shells of open section subjected to constrained torsion. Two structure solutions different in geometry are considered: open section cylindrical shell without stiffeners and reinforced by closed section stringers. The shells have five various length to diameter aspect ratio. Numerical simulations were carried out and the stress distribution in neuralgic zones in pre and post buckling response was determined. Torsion experiments were performed and the results were compared to the numerical solutions with a reasonably good agreement. The exactness of experiment for the chosen cases of considered solutions was proved by establishing the base for FEM numerical model estimation.

Key words: *shell, constrained torsion, open cross-section, post buckling, finite elements.*

1. INTRODUCTION

The tendency to design light-weight and high-strength structures, assuming the reasonable pay load to dead weight relation, has led to the constant research for more operative computation methods and new structures testing [1, 2]. It is related to the majority of technology areas, the thin-walled structures in particular. Durability and reliability of these structures are determined by presence of the neuralgic zones, necessary of utilitarian functions, on the other hand. These zones are some kind of local weakening or stress concentrators, introducing usually sudden variations of geometrical parameters. However, it is not difficult to provide the required torsional rigidity of closed section shell structures, but it is a considerably difficult

problem to meet this condition with reference to open section structures [3-7]. In such a case one of the most frequent methods to obtain the required torsional rigidity is to restrict the boundary conditions through clamping, at least, one free cross section end. As a result, besides shear stress in the cross-section, it appears the normal one as well. This kind of loading, defined as a constrained torsion, leads to the existence of high level stress gradients, at the free lengthwise border of shell in particular. It could cause the reduction of fatigue life and structure load capacity. Generally, it is necessary to strengthen the mentioned lengthwise boundaries, by closed cross-section stringers.

In this paper, the problem will be considered on the example of open section shell structures subjected to constrained torsion.

2. SUBJECT AND RANGE OF STUDY

The outline of considerations concerns numerical-experimental analysis of open cross-section thin-walled cylindrical shell subjected to constrained torsion. Two structure solutions different in geometry parameters are considered. The first is an open section cylindrical shell without stiffening. The second one represents the shell reinforced by three stringers of closed section.

Experimental investigations were performed together with numerical computations, for the two variants mentioned above: the shell without stiffening and the reinforced by three closed section stringers.

The installation scheme, loading device and structure dimensions with reinforcing stringers cross section are presented in Figure 1.

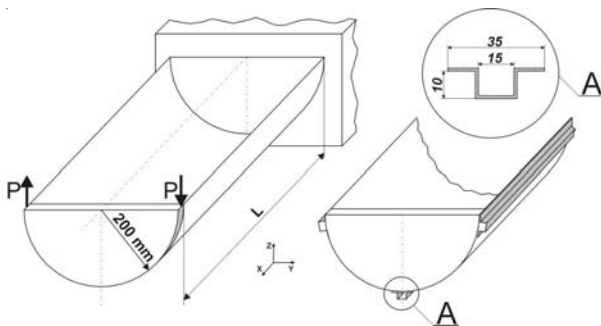


Fig.1 The installing scheme, directions of loading and dimensions of the cross section stringers

3. LINEARIZED PRE-BUCKLING ANALYSIS

Although an elastic buckling analysis of the structures generally represents a nonlinear problem in a number of cases being important from practical point of view, buckling analysis can be considered as a linear question.

The shells, considered in this study, were analysed with the ABACUS finite elements solver [8]. Using the bifurcation buckling analysis option, the linearized pre-buckling analysis was applied. The approach to buckling prediction is based on the development of a linear perturbation of the structure stiffness around an equilibrium solution point, which means the initial equilibrium under no load or preloaded state. At any time total elastic stiffness of the structure is:

$$[K]^0 + [K]^P \quad (1)$$

where $[K]^0$ is the stiffness caused by the material stiffness and $[K]^P$ is the initial stress and load stiffness caused by non-zero loading. For the elastic systems, $[K]^0$ is almost constant and the variation of $[K]^P$ is proportional to the load variation. During the bifurcation buckling step there may be a non-zero “dead” load P and there must be a linear perturbation load Q , specified in the bifurcation buckling step. The

quest of these considerations is to estimate the multiple of Q combined with P causing instability.

Since the response is assumed to be elastic and, therefore, closely proportional to the load, the stiffness at $P+\lambda Q$ load is well approximated by:

$$[K]^0 + [K]^P + \lambda [K]^Q \quad (2)$$

where $[K]^Q$ is the initial stress and load stiffness caused by Q . Thus, the buckling load estimation is provided by the eigenvalueproblem:

$$([K]^0 + [K]^P + \lambda [K]^Q)\phi = \{0\} \quad (3)$$

The eigenvalue λ is a multiplier of the applied load, which added to the preload, provides the critical load estimate: the predicted collapse load is $P+\lambda Q$ and ϕ is the collapse mode.

For the problems involving buckling behaviour, according to Refs. [8] and [9], the quadrilateral four-nodes, six degree of freedom shell elements were used in the models. Using MPC-TIE elements, the connections of skin and stringers in the points of rivet axes were made. In order to eliminate interpenetrating surfaces during eventual local buckling between rivets, very low stiffness solid elements were introduced into the space between the stringers and the skin. To define the boundary conditions corresponding to constrained torsion, translation degrees of freedom in the nodes of fixed boundary cross-section were blocked. Using MPC-PIN standard elements, the opposite boundary sections of shell were connected with 10 mm thickness stiff plates.

At the first step the calculations of structure without stiffeners were taken into consideration. The following constant materials were assumed: Young modulus $E=2.1 \cdot 10^5 \text{ N/mm}^2$ and Poisson’s ratio $\nu=0.3$. Assuming the constant shell diameter $D=200 \text{ mm}$, calculations were performed for five values of shell length: $L=200, 400, 600, 800$ and 1000 mm . In all cases the regular grid of structure partition for rectangular elements was assumed. The number of elements was increased repeatedly, according to the obtained results. In every geometry variant the same value of characteristic size grid - a , (see Figure 2) measured along the structure length was conserved. FEA shell models: without stiffeners - $L=200 \text{ mm}$ – minimal considered length, and with stiffeners - $L=1000 \text{ mm}$ – maximum considered length, are presented in Figure 2.

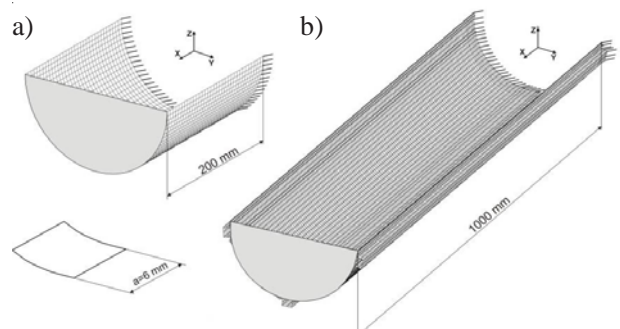


Fig. 2 Two examples of FEA shell models: a) shell without stiffeners, $L=200 \text{ mm}$; b) shell with stiffeners, $L=1000 \text{ mm}$

3.1 Structure without stiffening

In order to determine the stress distribution character in the shell without stiffening at pre-buckling state, numerical calculations were performed, for all geometry variants assuming the unitary external loading $M_t = 1 \text{ daNcm} = 102 \text{ Nmm}$. Figure 3 presents effective stress distribution according to von Mises criterion.

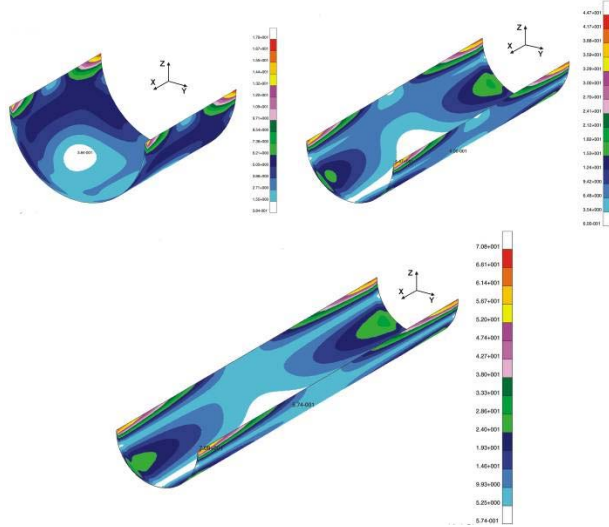


Fig. 3 Effective stress distribution according to von Mises criterion in the range of the pre-buckling state: the shells without stiffening: $L=200 \text{ mm}$, $L=600 \text{ mm}$, $L=1000 \text{ mm}$

Obtained results show that the highest stress levels and the largest gradient zones are located in the neighbourhood of unbounded longitudinal edges, in the areas adherent to boundary cross sections.

Using bifurcation buckling option critical load values and corresponding critical collapse modes were determined. In order to estimate the convergent solution in all variants the number of elements was achieved repeatedly.

On the basis of the obtained results we are able to present the relation between the critical buckling load M_{cr} versus length L of the shell for the considered geometry variants (Figure 4).

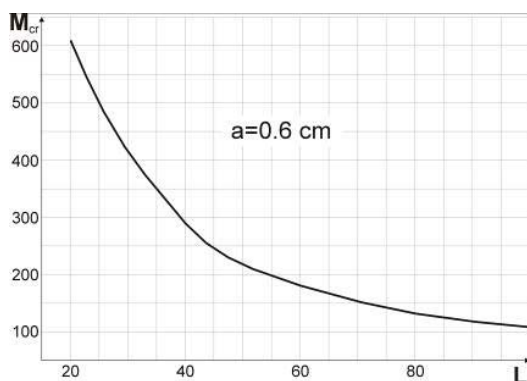


Fig. 4 The critical buckling load M_{cr} versus length L of the shell

Numerical results allow to present the shapes of the buckling modes. The first modes for the structures without stiffeners are presented in Figures 5, 6 and 7.

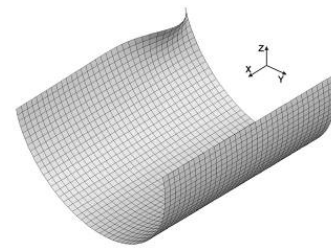


Fig. 5 First buckling mode, $L=400 \text{ mm}$, $M_{cr}=290.8 \text{ daNcm}$

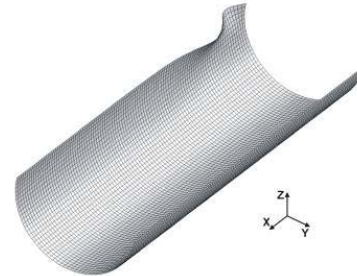


Fig. 6 First buckling mode, $L=600 \text{ mm}$, $M_{cr}=181.8 \text{ daNcm}$

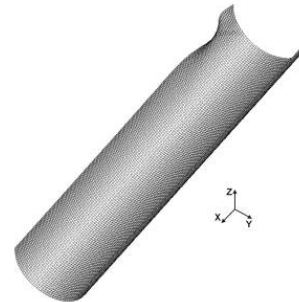


Fig. 7 First buckling mode, $L=1000 \text{ mm}$, $M_{cr}=106.0 \text{ daNcm}$

The results of calculation point out a strongly nonlinear relationship between critical moment and the length of shell, if the aspect ratio $L/D < 2$. Upwards the value sensitivity of critical moment does not grow much on the length increment.

3.2 The structures reinforced by stiffeners

Numerical results obtained for open section shells without stiffeners suggest that this kind of structures subjected to the constrained torsion do not have a practical application. It occurs due to too low critical local buckling level. This fact excludes the possibility of load increase over critical value in practice. Reinforcing the structure by stringers seems to be an effective method to increase stiffness and capacity. In our case the considered structures were reinforced by thin-wall stringers of closed section. This caused the increase of torsional stiffness, together with a slight structure weight growth. In each variant of the considered shells the same stringer cross section geometry, dimensions and their number were assumed. Analogically, as in case of shell without stiffeners, assuming the unitary external loading $M_t=1 \text{ daNcm}$, the character of the stress distribution in pre-buckling state was determined at the first step. The results of calculation in the form of effective stress distribution plots, according to von Mises criterion, are presented in Figures 8, 9 and 10.

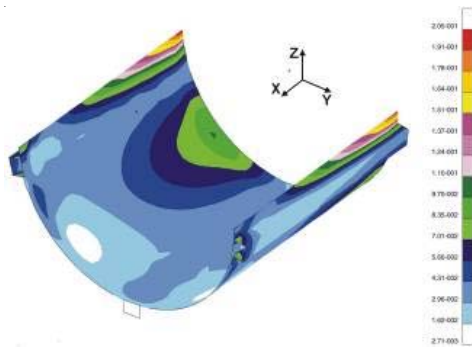


Fig. 8 Effective stress distribution, $L=200$ mm

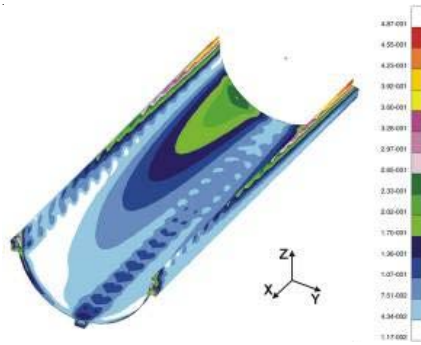


Fig. 9 Effective stress distribution, $L=600$ mm

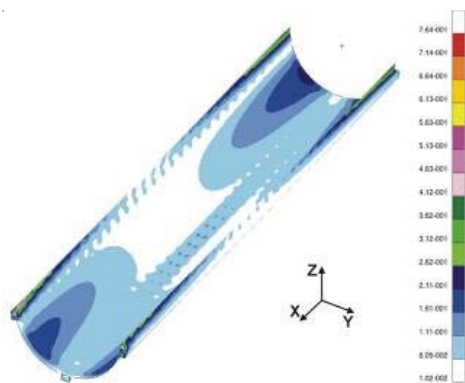


Fig. 10 Effective stress distribution, $L=1000$ mm

For structure geometry and the corresponding critical load from above, critical moments M_{Cr} and first buckling modes were determined. The shapes of the first buckling modes are presented in Figures 11, 12 and 13.

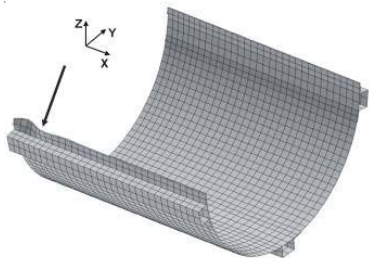


Fig. 11 First buckling mode, $L=200$ mm, $M_{Cr}=1841$ daNcm

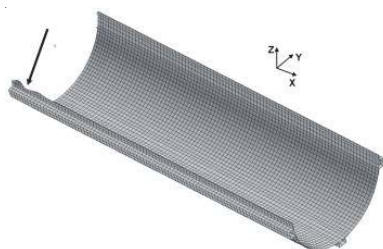


Fig. 12 First buckling mode, $L=600$ mm, $M_{Cr}=883$ daNcm

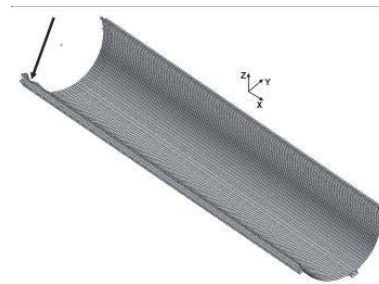


Fig. 13 First buckling mode, $L=1000$ mm, $M_{Cr}=827$ daNcm

Figure 14 presents the effect of length L on the buckling load M for the considered five geometry variants.

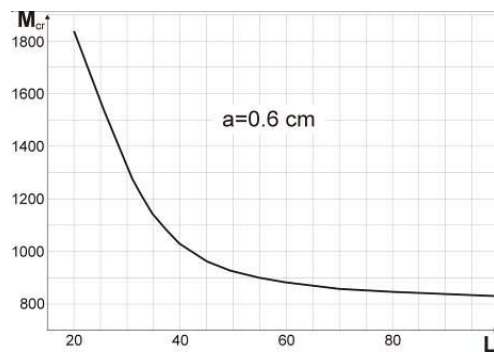


Fig. 14 The critical buckling load M_{Cr} versus length L of the shells

4. EXPERIMENTAL INVESTIGATIONS

Qualitative experimental research for selected variants of the considered structure was made parallel with numerical calculation. It allows to compare the buckling shape and critical load values obtained in the experimental and numerical way as well. The experiment was carried on the special station, enabling to perform the assumed loading and boundary conditions. Two cases were considered: the shell without reinforcement, and structure with three stringers of the closed section. In both cases the specimen length was $L=1000$ mm. The Figure 15 presents the scheme of the station.

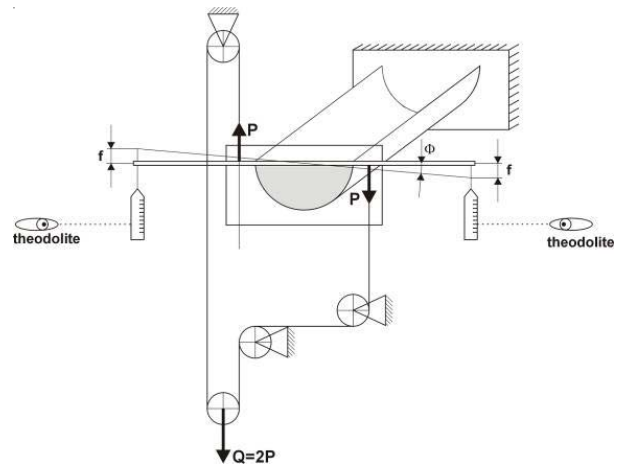


Fig. 15 The scheme of station

Structure stiffness measurements in the pre-buckling state range preceded buckling investigation. Figure 16 presents the plot of torsion angle versus torsion moment.

Characteristics presented in Figure 16 show, in the range of pre-buckling load, that the relationship between torsion moment and torsion angle is linear exactly up to the moment on abrupt structure stiffness variation.

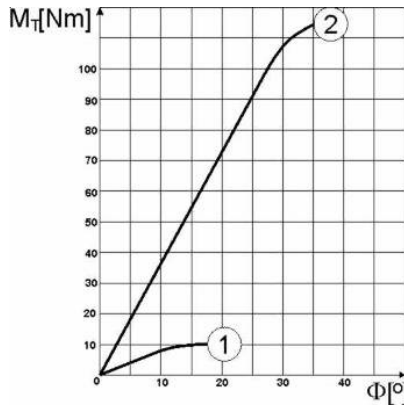


Fig. 16 Torsion moment versus torque angle:
1 - shell without reinforcement, 2 - structure with stiffeners

Figure 17 presents local buckling shape of the shell without reinforcement noticed during experimental investigation. In this case critical moment was $M_{cr}^e \approx 125 \text{ daNcm}$, while the numerical result was $M_{cr} = 106 \text{ daNcm}$. Quantitative comparison of both results suggests a reasonably good compatibility (~15%).

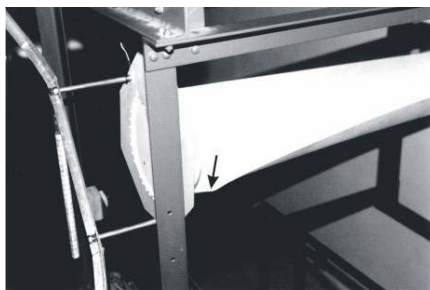


Fig. 17 Local buckling of the structure without reinforcement,
 $L=100 \text{ cm}$

The similar statement can be formulated with reference to the reinforced structure. In this case the critical loading obtained on the experimental way outnumbered numerical results as well. Figure 18 presents post buckling deformation.



Fig. 18 Post-buckling plastic deformation: structure reinforced by closed section stiffeners

The presented effects of experimental studies show that the structures considered are characterised not only by the low torsional rigidity, but also by large deformations. Therefore, an application of the linear FEM analysis can refer to the undercritical deformation range only. It enables to identify stress concentration zones, possible local buckling areas.

In order to determine the stress distribution in post buckling state, the nonlinear static analysis was performed. The stress-strain relation of uniaxial tension for real material was simplified by the model of the ideal elastic-plastic body with yield point 240 MPa (Figure 19).

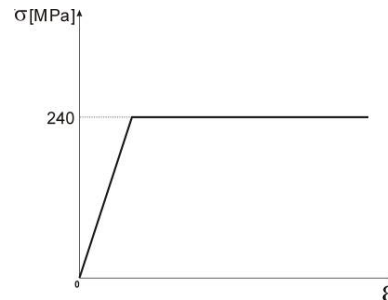


Fig. 19 Physical characteristics of the material

5. NON-LINEAR FEM ANALYSIS

The results of experimental studies showed that even small load increment over the critical value leads to the structure local plastic deformation. The numerical simulation of post buckling deformation phenomena requires a non-linear procedure application. Large deformations and the change of the structure rigidity have to be taken into consideration.

Non-linear formulation of the problem leads to the discrete equilibrium equations encountered in non-linear static structural analysis, formulated by the displacement method presented in the compact force residual form [10]:

$$\mathbf{r}(\mathbf{u}, \mathbf{A}) = \mathbf{0} \quad (4)$$

Here \mathbf{u} is the state vector, containing the degrees of freedom, that characterize the configuration of the structure, \mathbf{A} is an array of control parameters, containing the components of external loading, whereas \mathbf{r} is the residual vector containing out-of-balance forces conjugate to \mathbf{u} . Varying the vector \mathbf{r} with respect to the components of \mathbf{u} in assumption - $\mathbf{A} = \text{constant}$, tangent stiffness matrix \mathbf{K} in structural mechanics application can be written as:

$$\mathbf{K} = \frac{\partial \mathbf{r}}{\partial \mathbf{u}} \quad (5)$$

An alternative version of Eq. (5) is the force-balance form:

$$\mathbf{p}(\mathbf{u}) = \mathbf{f}(\mathbf{u}, \mathbf{A}) \quad (6)$$

The \mathbf{p} vector contains components of internal forces, resulting from deformation of the structure; however \mathbf{f} are the control-dependent external forces,

posing the set introduced respectively during the next stages of the analysis, which are also able to be dependent on current geometry of the structure.

Philosophy of the non-linear analysis in FEM is based on the gradual application of control parameters, realized in the next stages. It corresponds to the stage for every reliable state of the structure, in which a static balance is specific to correspond to the solution of Eq. (4). Control parameters connected to external forces components are expressed, in general, as functions of reliable quantity λ , called the stage control parameter. The result of the non-linear analysis poses the set of solutions, corresponding to each values of the λ parameter. They create the equilibrium path of the system. The unambiguous graphical interpretation of the equilibrium path is possible for at most two degrees of freedom. However on the basis of the external loading knowledge, the value of stage control parameters and related geometric configurations of the structure, it is possible to obtain an approximated dependence between selected values describing deformation of the structure versus external loading. In the cases of the considered numerical model, equilibrium paths were determined into the system: torsional moment versus total torsional angle.

Algorithms of non-linear analysis are based, mainly, on iterative and incremental - iterative procedures. The stiffness matrix K is treated in every solution stage as a constant and it is experiencing the increase as far, as λ stage control parameter grows. Newton - Raphson algorithm constitutes the basic iterative method. The lack of chance to obtain the solution convergence is the method defect. It is bound up with the appearance of the limit of bifurcation points on the equilibrium path. In such situations the arc length method is applied, which makes possible to determine the balance of the system [11-15].

In the considered problem, applying MSC MARC 2005 programme [16], non-linear numerical analyses were performed. This programme is creating the chance of the user's meaning intervention in the issue of iteration parameters selection.

The same numerical model, which was applied to the linear analysis, was utilized without stiffening stringers as a structure. Two diversified numerical models were analyzed, with structure stiffened by the stringers of "omega" cross-section each. The first one has the skin - stringer rivet joint simulated by beam elements. A contact was also reflected between surfaces of stringers and the skin. A simplification was applied to the second model, relying on the continuous connection of stringers with skin. The model of the first version consisted of 16109 four-nodes shell elements, when every node contained 6 degrees of freedom. The model of the second version consisted of 6724 shell elements of the same type.

Effects illustrating the character to deformation of numerical examinations and effective stress distribution on external surfaces of structures were presented in Figures from 20 to 25.

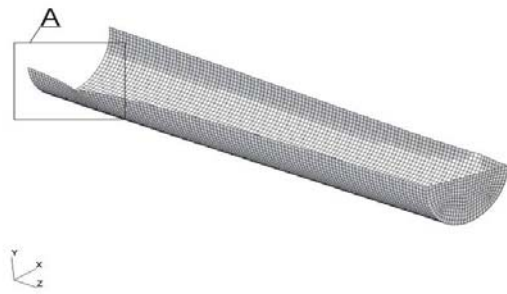


Fig. 20 Post buckling deformation: structure without stringers

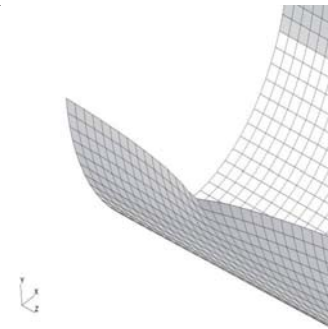


Fig. 21 Form of post buckling deformation in area of A detail, real scale

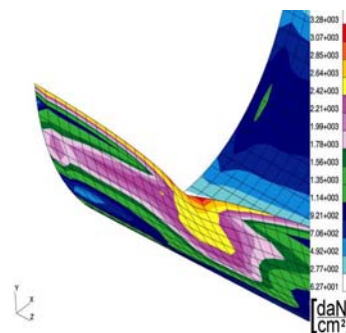


Fig. 22 Effective stress distribution according to von Mises criterion on external surface

The results of calculations presented in Figures 20 to 22 prove the existence of local plastic deformation areas in the neighbourhood of boundary fixing of the structure. These effects show satisfactory compatibility with the experiment (compare Figure 17), both in bringing back to the location and the character of the plastic deformation range.



Fig. 23 Version 1- riveted joint of the skin with the stringer, local post buckling deformation

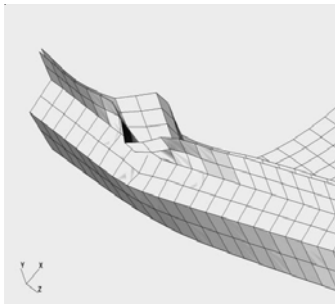


Fig. 24 Form of local deformation, detail C

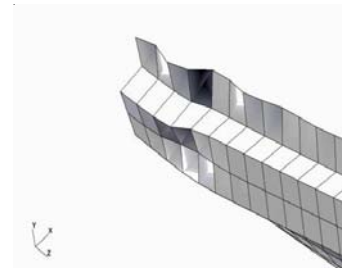


Fig. 27 Character of deformation, detail B

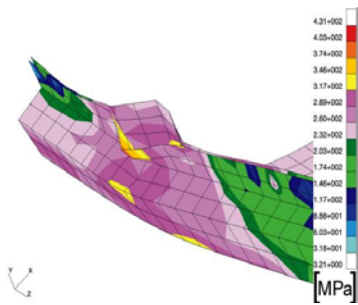


Fig. 25 Effective stress distribution according to von Mises criterion, on external surfaces

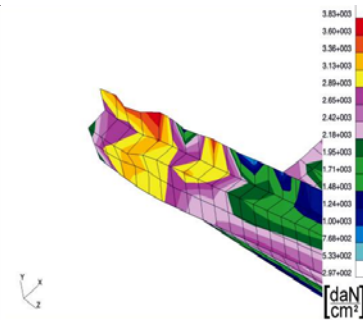


Fig. 28 Effective stress distribution on external surface, according to von Mises criterion

Figures 23 to 25 present numerical results for the model, where the connection was reflected by rivets. The received result, describing the state of local plastic deformation in post buckling state, differs from the effect received in the experimental way, under quality consideration. A lot of attempts were done (not presented here) to identify the reasons for the received divergence of effects. It is possible, on this basis, to make an attempt to explain this phenomenon.

Looking at Figure 25, the elements of the skin and stringer in the zone between rivets were subjected to transverse dislocations moving in opposite directions, while direction of dislocations in the experiment was the same. This divergence could be the result of loss of stability bifurcation character. A reasonable suggestion comes from the fact that in both elements the bifurcation had the stable-symmetrical character. In the real structure, geometric imperfections could decide about the identical direction of both surfaces dislocation already initiated during the riveting process.

The second model turned out to be interesting (Figures 26-28). The effects of numerical calculations correspond exactly to the results received in the experimental way. The applied simplifications adjust conditions of the iteration parameters selection in the real structure transformation. They rely on a continuous connection between stringers and skin surfaces that eliminates the chance to receive local stress concentration in the proximity of rivets. It is possible to regard the received results satisfactory if we consider the character of the received advanced plastic deformation and responding stress distribution.

In Figure 29 the relationship between the torsion moment and the torsion angle obtained in experimental and numerical ways is presented.

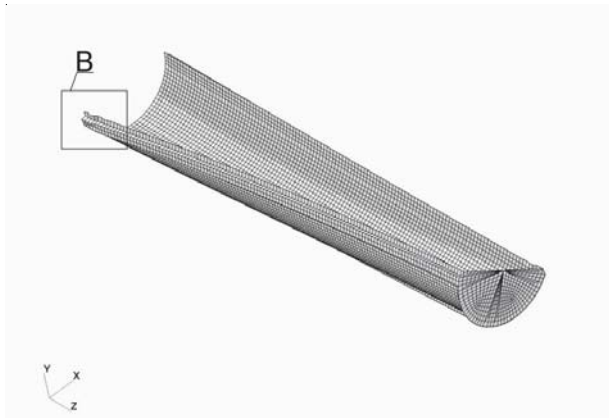


Fig. 26 Version 2 - continuous connection of skin and stringers, local post buckling deformation

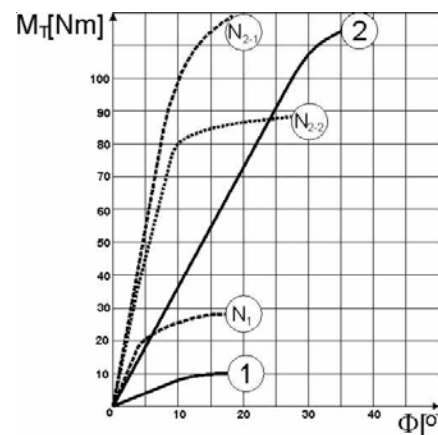


Fig. 29 Relationship between the torque moment versus the torsional angle; 1 - Structure without stringers – experimental result; 2 - Structure reinforced by closed section stiffeners – experimental result; N_1 - Structure without stringers – numerical result; $N_{2.1}$ - Version of continuous connection of skin and stringers – numerical results; $N_{2.2}$ - Version of riveted joint of the skin with the stringers – numerical results

It is necessary to underline that the effects of numerical calculations present approximate relations between the loading and the accepted parameter determining the structure deformation. In fact, the obtained characteristics express the relationship between the torsion angle of the structure and the product $M_{max} \cdot p_t$, where p_t denotes pseudo-time coefficient, as the step of load advantage application in the particular step of counts, whereas M_{max} is the maximum value of the structure loading. In the considered case, it is a maximum value of the torsional moment. The relationship is dependent on the accepted method of the solution, parameters of the iteration and the shape of the equilibrium path between the products mentioned above and the real loading of the numerical model. Let us notice that the loading of the numerical model is the maximum accepted value of the torsional moment for $p_t=1$.

6. CONCLUDING REMARKS

On the basis of the numerical and experimental results several statements essential for engineering practice could be formulated:

- The results obtained in the numerical way show higher critical load values in all considered cases. It is possible to explain it by not a very precise rigidity reflecting the real design in the numerical model as the whole. It is related to the plates boundary conditions reflecting in particular. The structure stiffness development process is not without meaning too.
- Received divergence of the nonlinear numerical analysis with the results of experimental studies suggests the necessity of taking into consideration appropriate imperfections of structure geometry in the numerical model. Received effects would be able to pose reliable hints, not to say requirements in relation to the technological process, in particular neuralgic zones determining the load capacity of structure.
- Presented investigations denoted experimental revision, an information source about structure behaviour under loading that performs verification function for numerical FEM model in particular, when the solution of the problem requires a nonlinear formulation.

7. REFERENCES

- [1] J. Arbocz, Shell Stability Analysis: Theory and Practice, In: Collapse: The buckling of structures in theory and practice, Eds. J.M.T. Thompson and G.W. Hunt G.W., pp. 43-74, Cambridge University Press, 1983.
- [2] O.C. Zienkiewicz and R.L Taylor, *Finite Element Method For Solid and Structural Mechanics*, Elsevier Butterworth-Heinemann, Oxford, 2005.
- [3] G.P. Dube and P.C. Dumir, Tapered thin open section beams on elastic foundation – Part I: Buckling analysis, *Comp. & Struct.*, Vol. 61, pp. 845-857, 1995.
- [4] M. Królak and A. Mlotkowski, Experimental analysis of post-buckling and collapse behaviour of thin-walled box-section beam, *Thin Wall Struct.*, Vol. 26, pp. 287-314, 1996.
- [5] L. P. Kollar, Flexural-torsional buckling of open section composite columns with shear deformation, *Int. J. Solids Struct.*, Vol. 38, pp. 7525-7541, 2001.
- [6] F. Mohri, L. Azrar and M. Potier-Ferry, Flexural-torsional post buckling analysis of thin-walled elements with open sections, *Thin Wall Struct.*, Vol. 39, pp. 907-938, 2001.
- [7] F. Mohri, L. Azrar and M. Potier-Ferry, Lateral post buckling analysis of thin-walled open section beams, *Thin Wall Struct.*, Vol. 40, pp. 1013-1036, 2002.
- [8] ABAQUS Analysis, User's Manual, version 6.3, Hibbit, Karlsson & Sorensen Inc., 2002.
- [9] K.J. Bathe, *Finite Element Procedures*, Prentice Hall, Upper Saddle River, New Jersey, 1996.
- [10] C.A. Felippa, *Nonlinear Finite Element Methods*, Department of Aerospace Engineering Sciences, University of Colorado, Boulder, 2004.
- [11] M.A. Crisfield, A faster modified Newton-Raphson iteration, *Comp. Meth. Appl. Mech. Eng.*, Vol. 20, pp. 267-278, 1979.
- [12] M.A. Crisfield, Incremental/iterative solution procedure for nonlinear structural analysis, In: Numerical Method for Nonlinear Problems, Vol. 1, Eds. C. Taylor, E. Hinton and D.R.J. Owen, pp. 261-290, Pineridge Press, Swansea, 1980.
- [13] M.A. Crisfield, An arc-length method including line searches and accelerations, *Int. J. Num. Meth. Eng.*, Vol. 19, pp. 1269-1289, 1983.
- [14] E. Riks, An incremental approach to the solution of snapping and buckling problems, *Int. J. Solids Struct.*, Vol. 15, pp. 329-351, 1979.
- [15] E. Riks, Some computational aspects of the stability analysis of nonlinear structures, *Comp. Meth. Appl. Mech. Eng.*, Vol. 47, pp. 219-260, 1984.
- [16] MSC MARC FE, User's Manual, 2005.

STANJE NAPREZANJA NAKON IZVIJANJA OTVORENIH CILINDRIČNIH LJUSKI IZLOŽENIH OGRANIČENOJ TORZIJI

SAŽETAK

Ovaj se rad bavi numeričkim i eksperimentalnim proučavanjem stanja otvorenih cilindričnih ljuski, tankih čeličnih stijenki prije i poslije izvijanja izloženih ograničenoj torziji. Razmatraju se dva konstrukcijska rješenja različite geometrije: otvorene cilindrične ljuske bez ojačanja i otvorene cilindrične ljuske ojačane zatvorenom ukrutom. Ljuske imaju pet različitih duljina prema omjeru promjera. Napravljene su numeričke simulacije i određena je preraspodjela napreznja na neuralgičnim zonama prije i poslije izvijanja. Napravljene su eksperimenti s torzijom te su se rezultati usporedili s numeričkim rješenjima što je pokazalo sasvim dobru podudarnost. Dokazana je točnost eksperimenta u odabranim slučajevima promatranih rješenja tako da je uspostavljena baza za procjenu numeričkog modela po metodi konačnih elemenata.

Ključne riječi: ljuska, ograničena torzija, otvoreni poprečni presjek, stanje nakon izvijanja, konačni elementi.